

# Journal of Materials Chemistry A

Accepted Manuscript



This is an *Accepted Manuscript*, which has been through the Royal Society of Chemistry peer review process and has been accepted for publication.

*Accepted Manuscripts* are published online shortly after acceptance, before technical editing, formatting and proof reading. Using this free service, authors can make their results available to the community, in citable form, before we publish the edited article. We will replace this *Accepted Manuscript* with the edited and formatted *Advance Article* as soon as it is available.

You can find more information about *Accepted Manuscripts* in the [Information for Authors](#).

Please note that technical editing may introduce minor changes to the text and/or graphics, which may alter content. The journal's standard [Terms & Conditions](#) and the [Ethical guidelines](#) still apply. In no event shall the Royal Society of Chemistry be held responsible for any errors or omissions in this *Accepted Manuscript* or any consequences arising from the use of any information it contains.

# Highly Enhanced Lithium Storage Capability of $\text{LiNi}_{0.5}\text{Mn}_{1.5}\text{O}_4$ by Coating with $\text{Li}_2\text{TiO}_3$ for Li-ion Batteries

Cite this: DOI: 10.1039/x0xx00000x

Haifu Deng, Ping Nie, Haifeng Luo, Yi Zhang, Jie Wang, and Xiaogang Zhang\*

Received 00th January 2012,  
Accepted 00th January 2012

DOI: 10.1039/x0xx00000x

www.rsc.org/

A uniform and thin  $\text{Li}_2\text{TiO}_3$  layer with various amounts was coated on the surface of nanostructured  $\text{LiNi}_{0.5}\text{Mn}_{1.5}\text{O}_4$  (LNMO) materials by *in situ* hydrolysis of tetrabutyl titanate (TBOT) followed by lithiation process. The morphology and structure of the samples were investigated by X-ray diffraction (XRD) and transmission electron microscopy (TEM) with an energy-dispersive X-ray spectroscopy (EDS). Electrochemical tests illustrate that  $\text{Li}_2\text{TiO}_3$  as  $\text{Li}^+$ -conductive coating remarkably improved the rate and cycling performance of LNMO spinel cathode. Particularly, the 3 wt. % and 5 wt. %  $\text{Li}_2\text{TiO}_3$ -surface modified samples deliver high discharge capacity of  $95 \text{ mAh g}^{-1}$  and  $90 \text{ mAh g}^{-1}$  even at a high current density of 5 C, while the bare one only has a discharge capacity of  $70 \text{ mAh g}^{-1}$ . At a current density of 1 C at elevated temperature, the 3 wt. % and 5 wt. %  $\text{Li}_2\text{TiO}_3$ -surface modified LNMO samples show excellent cyclability. After 50 cycles, the capacity retention of 3 wt. % and 5 wt. %  $\text{Li}_2\text{TiO}_3$  modified LNMO is 88.1% and 94.1%, while only 77.1% for the bare sample.

## 1. Introduction

Nowadays, the threats caused by energy shortage, environmental pollution and climate change become increasingly obvious. The demands for renewable and clean energy are going up continually.<sup>1-2</sup> To fulfill these requirements, Li-ion batteries (LIBs) with high energy efficiency, low cost and long cycle life have gained enormous attentions.<sup>3-6</sup> At present, LIBs have been widely used in portable electronic devices, such as mobile phones, cameras and laptops. However, the application of LIBs for electric vehicles (EVs) or renewable energy storage is largely limited due to the finite energy/power density. Substantial research indicates that the energy/power is mainly limited by the cathode material and intensive attempts have been made to develop cathode materials with large capacity or high voltage.<sup>7-10</sup> In this regard, spinel LNMO has attracted much interest owing to its high operating voltage and relatively high theoretical capacity ( $147 \text{ mAh g}^{-1}$ ).<sup>11-14</sup> Moreover, LNMO shows markedly improved cycling performance at ambient temperature compared to  $\text{LiMn}_2\text{O}_4$  because that it could effectively suppress the dissolution of  $\text{Mn}^{3+}$  and Jahn-Teller distortion.<sup>15</sup> Recently, Jafta *et al* prepared nanostructured  $\text{LiMn}_{1.5}\text{Ni}_{0.5}\text{O}_4$  spinel through microwave-assisted synthesis and it exhibits excellent electrochemical performance.<sup>16</sup>

Unfortunately, the operation voltage of LNMO exceeds the superior voltage limit of the conventional electrolyte constituting  $\text{LiPF}_6$  solute and carbonate solvent. At such a high voltage ( $\sim 4.7 \text{ V}$ ), undesired oxidative decomposition of electrolyte occurs during charging process and the corresponding products would cover on the surface of LNMO cathode, forming a cathode electrolyte interphase (CEI) with

poor conductivity.<sup>17, 18</sup> At room temperature, this side reaction is relatively slow, the cathode exhibits preferable cyclability in a short course of circulation. However, when the temperature is close to  $55 \text{ }^\circ\text{C}$ , the electrolyte oxidation becomes severely serious. During charge-discharge cyclic process, the CEI film is constantly thickening and LNMO spinel undergoes severe capacity fade.

In order to improve the cycle performance of this material, many efforts have been devoted to addressing these challenges.<sup>19</sup> High potential electrolytes with better electrochemical stability in a wider voltage range have been developed.<sup>20, 21</sup> Moreover, multiple surface coatings have been explored, such as  $\text{SiO}_2$ ,  $\text{ZrO}_2$ ,  $\text{ZnO}$ ,  $\text{Al}_2\text{O}_3$ ,  $\text{AlF}_3$  and  $\text{FePO}_4$ .<sup>22, 23</sup> In addition, some dopant cations (Cr, Fe, and Ga) could segregate preferentially to the surface of LNMO, resulting in a more stable cathode-electrolyte interface and better cyclability.<sup>24, 25</sup>

Among these modifications, surface coating which could stabilize the surface structure of cathode materials has been considered as one of the most effectively ways to ameliorate the electrochemical performance of the spinel. Nevertheless, a majority of oxide coatings are usually poor conductors of lithium and electron, which may bring some negative effect to the rate performance. Recently, solid electrolytes with excellent ionic conductivity have been chosen as the surface cladding. Song *et al* employed polyimide (PI) to wrap the surface of LNMO.<sup>26</sup> Compared to conventional metal oxide-based coatings, the unusual PI wrapping layer could offer facile ion transport channels. Zhou *et al* selected  $\text{LiAlO}_2$  as lithium-containing surface coating layer of LNMO.<sup>27</sup> The results showed that both rate performance and cycling stability were markedly enhanced.

Lithium titanate ( $\text{Li}_2\text{TiO}_3$ ) has attracted many researchers' attentions for its three-dimensional  $\text{Li}^+$ -ion diffusion path and outstanding structural stability in organic electrolyte, which is capable of stabilizing the structure of high-capacity cathode materials and suitable to be chosen as coating layer for cathode.<sup>28</sup> Moreover, the lithium ionic conductivity of  $\text{Li}_2\text{TiO}_3$  would be greatly increased when doped with foreign ions, resulting from the formation of vacancies.<sup>29-31</sup> In this work,  $\text{Li}^+$ -conductive  $\text{Li}_2\text{TiO}_3$  has been employed to coat on the surface of LNMO cathode. The  $\text{Li}_2\text{TiO}_3$ -modified LNMO samples were prepared by two-step strategy that involves *in situ* hydrolysis of tetrabutyl titanate (TBOT) on the LNMO nanoparticles which could achieve uniform  $\text{Li}_2\text{TiO}_3$ -precursor coating and subsequent lithiation process with  $\text{Li}_2\text{CO}_3$ . It should be noted that the nanoarchitectured  $\text{Li}_2\text{TiO}_3$  layer could provide facile ion transport channels and suppress the formation of thick CEI layers. The effect of the amount of  $\text{Li}_2\text{TiO}_3$  on the electrochemical properties was also extensively investigated.

## 2. Experimental

### 2.1 Materials Synthesis.

The bare LNMO sample was synthesized by resorcinol-formaldehyde assisted synthesis. 0.1 mol resorcinol and 0.15 mol formaldehyde were dissolved in 100 ml distilled water. Afterwards, 0.0206 mol  $\text{LiCH}_3\text{COO}\cdot 2\text{H}_2\text{O}$ , 0.01 mol  $\text{Ni}(\text{CH}_3\text{COO})_2\cdot 4\text{H}_2\text{O}$  and 0.03 mol  $\text{Mn}(\text{CH}_3\text{COO})_2\cdot 4\text{H}_2\text{O}$  were added respectively. Then the resultant mixture was heated at 60 °C until viscous and the green gel was formed. Finally, nano-LNMO was obtained by calcination of the obtained products at 750 °C for 12 h under air.

To prepare  $\text{Li}_2\text{TiO}_3$  surface modified LNMO sample, the above-synthesized nano-LNMO was dispersed in ethyl alcohol containing small amounts of aqueous ammonia. And then  $\text{Ti}(\text{OC}_4\text{H}_9)_4$  dissolved into ethanol beforehand was dropped in the suspension. The mixture was maintained at 45 °C for 24 h and TBOT hydrolyzed slowly. After that, the solvent was evaporated at 60 °C and the solid powder was heated at 400 °C. Eventually, stoichiometric amounts of  $\text{Li}_2\text{CO}_3$  (corresponding to  $\text{Li}_2\text{TiO}_3$ ) was mixed thoroughly and the mixture was calcinated at 800 °C for 3 h.

### 2.2 Materials Characterization.

The crystal structure of as-prepared samples were characterized by X-ray diffraction (XRD, Bruker D8 with  $\text{Cu K}\alpha$  radiation) in scan rate of  $3^\circ \text{min}^{-1}$  over  $10^\circ$  to  $80^\circ$   $2\theta$  range. The morphologies and structural features of the samples were examined by high-resolution transmission electron microscopy (TEM, JEOL JEM-2100). Scanning transmission electron microscopy (STEM) was carried out with Tecnai G2 F30 S-TWIN. The X-ray photoelectron spectroscopy (XPS) analysis was performed on a Perkin-Elmer PHI 550 spectrometer with  $\text{Al K}\alpha$  (1486.6 eV) as the X-ray source.

In order to analyze the electrochemical properties of the samples, CR2016-type coin cell was employed to carry out galvanostatic cycling tests. The working electrodes were prepared by mixing 80 wt.% LNMO active materials, 10 wt.% carbon black, 10 wt.% polyvinylidene fluorides (PVDF) in N-methyl pyrrolidinone (NMP) to form homogenous slurry. The mixture was uniformly coated on the aluminum foil current collector and dried under vacuum at 110 °C for 12 h. The mass loading of active material is about  $1.6\text{-}2\text{mg cm}^{-2}$ . Lithium metal

was used as anode and polypropylene (PP) film was acted as separator. The electrolyte was 1.0 M  $\text{LiPF}_6$  in a 1:1 mixture solution of ethylene carbonate and dimethyl carbonate. Coin cells were assembled in a glove box under argon atmosphere. Galvanostatic tests were performed at different current densities between 3.2 and 5 V (vs.  $\text{Li/Li}^+$ ) using a CT2001A cell test instrument (LAND Electronic Co.). Electrochemical impedance spectroscopy (EIS) data were collected in a frequency range from 100 kHz to 0.01 Hz with an AC amplitude of 5 mV on a CHI660C electrochemical workstation (Chenhua, Shanghai).

## 3. Results and discussion

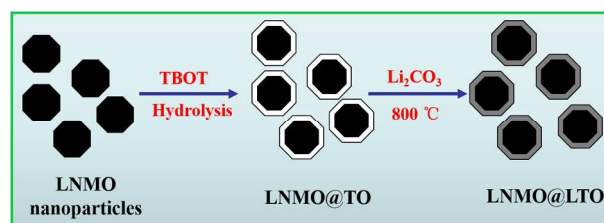


**Figure 1.** Illustration of the approach for surface modified  $\text{Li}_2\text{TiO}_3$ -LNMO nanoparticles.

The synthetic process of the  $\text{Li}_2\text{TiO}_3$ -LNMO nanoparticles (LNMO@LTO) contains two steps, in which  $\text{TiO}_2$ -coated LNMO nanoparticles (LNMO@TO) were first prepared through TBOT-hydrolysis procedure followed by 400 °C heat treatment, and then they were mixed with  $\text{Li}_2\text{CO}_3$  and lithiated to obtain the coated products (Figure 1). LNMO nanoparticles prepared through resorcinol-formaldehyde assisted method were chosen as the precursors, owing to their nano structures with small particle size are propitious to be uniformly coated. Samples with progressive proportion of  $\text{Li}_2\text{TiO}_3$  were obtained by adjusting the amount of TBOT. The LNMO@LTO composites with 3, 5, and 10 wt.%  $\text{Li}_2\text{TiO}_3$  were referred as LNMO@LTO 3%, LNMO@LTO 5% and LNMO@LTO 10%, respectively.

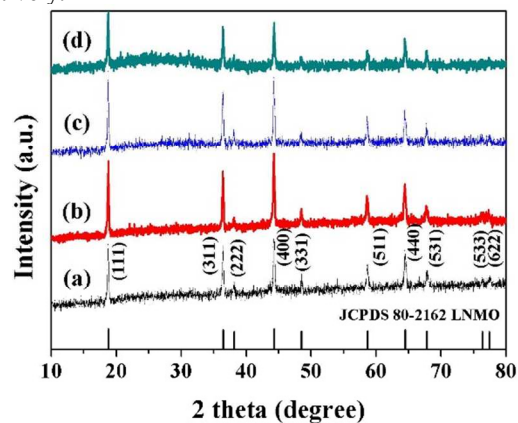


**Figure 2.** XRD patterns of pristine LNMO and LNMO@LTO cathode materials: (a) LNMO; (b) LNMO@LTO 3%; (c) LNMO@LTO 5%; (d) LNMO@LTO 10%.

Figure 2 compares the XRD patterns of the bare and  $\text{Li}_2\text{TiO}_3$ -surface modified LNMO samples. All patterns can be assigned to well crystallized cubic spinel LNMO (JCPDS Card No. 80-2162), indicating that  $\text{Li}_2\text{TiO}_3$  incorporation does not change the structure.<sup>32,33</sup> No diffraction peaks from  $\text{Li}_2\text{TiO}_3$  are observed, probably due to that the relatively low loading content and layered  $\text{Li}[\text{Ni}_x\text{Mn}_y\text{Ti}_z]\text{O}_2$  domains in the surface layer of  $\text{Li}_2\text{TiO}_3$ .<sup>30,31</sup> In order to further illustrate the components of

surface coating, the proportion of  $\text{Li}_2\text{TiO}_3$  in LNMO@LTO complex was increased to 20 wt. % (LNMO@LTO 20%). Besides, pure  $\text{Li}_2\text{TiO}_3$  was prepared through the similar manner and the XRD pattern can be perfectly indexed to  $\text{Li}_2\text{TiO}_3$  (JCPDS Card No.33-0831).<sup>34</sup> As shown in the Figure S 1, different from the bare LNMO, characteristic peaks for  $\text{Li}_2\text{TiO}_3$  around  $43.58^\circ$  and  $63.48^\circ$  began to appear in the XRD pattern of LNMO@LTO 20% (marked by small black square). In addition, as illustrated in Table S 1, the calculated lattice parameters and unit cell volume of LNMO@LTO became greater with the increase of LTO content, suggesting that  $\text{Ti}^{4+}$  ions would migrate from surface into the spinel structure as doping ions, which is in agreement with the fact that the ionic radius of  $\text{Ti}^{4+}$  (74.5 pm) is much larger than that of  $\text{Mn}^{4+}$  (67 pm).<sup>35, 36</sup>

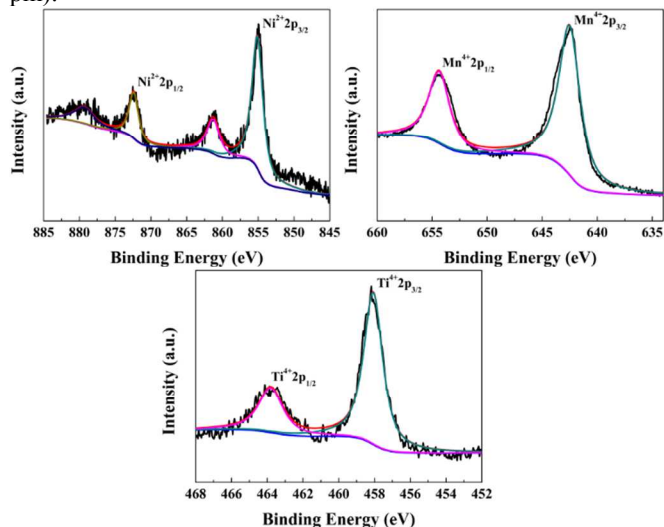


**Figure 3.** XPS spectra for Ni, Mn and Ti elements of LNMO@LTO 5% sample.

XPS experiments were performed for the coated spinel sample to further evaluate the surface structure of LNMO after  $\text{Li}_2\text{TiO}_3$ -modification. Figure 3 shows the XPS spectra for Ni, Mn and Ti elements of LNMO@LTO 5% sample. The valences of Ni, Mn and Ti are determined to be +2, +4, +4, respectively.<sup>28, 30</sup> Moreover, as for the precursor applied in the synthetic process of LNMO@LTO 5%, the atomic ratio of Ti to (Ni + Mn) is 5: (36+100), while that of LNMO@LTO 5% is 20: (30+100), which suggests  $\text{Ni}^{2+}$  or  $\text{Mn}^{4+}$  would diffuse from the core to the shell, resulting in the formation of  $\text{Li}_2\text{Ti}_{1-y}\text{M}_y\text{O}_3$  ( $\text{M}=\text{Mn}, \text{Ni}$ ) or layered  $\text{Li}[\text{Ni}_x\text{Mn}_y\text{Ti}_z]\text{O}_2$  domains in the surface layer of  $\text{Li}_2\text{TiO}_3$  and  $\text{Li}_2\text{TiO}_3$ -rich coating layer was formed on the surface of LNMO nanoparticles indeed.<sup>30, 31</sup> It should be expected that the ionic conductivity of  $\text{Li}_2\text{TiO}_3$  would be increased when doped with foreign ions (Ni or Mn) and the rate capability of LNMO will be enhanced by the doped- $\text{Li}_2\text{TiO}_3$  coating.

The morphology and structure of pristine LNMO and LNMO@LTO 5% cathode materials were confirmed by TEM. As shown in Figure 4a, b, LNMO nanoparticles with an average particle size ranging between 100-200 nm were successfully prepared and the pristine LNMO has smooth planes and well-defined edges. Figure 4c, d shows the TEM images of LNMO@LTO (5%). After modifications, a thin and highly continuous coating was covered on the surface of pristine LNMO. Elemental mapping for Ni, Mn and Ti shows that all the elements are distributed homogeneously throughout the nanoparticles, indicating that the obtained materials were coated

by  $\text{Li}_2\text{TiO}_3$  uniformly (Figure 4 f-h). However, there is hardly any segregation on a scale below the resolution of the EDS technique and the thickness uniformity of coatings could not be obtained. The thickness of coating layer could be analyzed perfectly by a high-resolution image or electron energy loss spectroscopy (EELS) mapping.<sup>37, 38</sup>

The discrepancy in crystal structures between the core and shell was evidently demonstrated by a high-resolution (HR) TEM image (Figure 4i) of the black frame region in Figure 4d. The d-spacing of coating layer is 0.480 nm, which is well matched with the d-spacing of (002) plane for the standard monoclinic  $\text{Li}_2\text{TiO}_3$ <sup>31</sup>, further suggesting a successful formation of the hierarchical LNMO@LTO as desired. Moreover, it is evident from Figure 4i that the  $\text{Li}_2\text{TiO}_3$  coating layers with the thickness of approximately 8 nm are distributed on the particle surfaces, which can effectively segregate LNMO from liquid electrolyte.

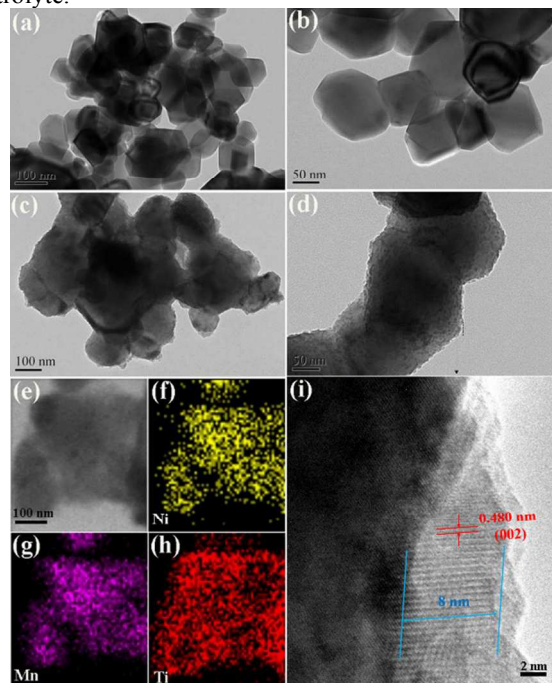


**Figure 4.** TEM images of LNMO (a, b) and LNMO@LTO 5% (c, d); STEM image of LNMO@LTO 5% (e) and element mapping of Ni (f), Mn (g), Ti (h); HRTEM image of black frame region in Figure 4d for LNMO@LTO 5% (i).

To evaluate the electrochemical performance of LNMO@LTO, CR2016 coin cells were assembled with Li metal as counter electrodes. Meanwhile, bare LNMO sample was also tested in the same condition for comparison. Figure S 2 shows the typical galvanostatic charge/discharge curves of the four samples tested at a current rate of 0.1C ( $1\text{C} = 147 \text{ mAh g}^{-1}$ ) within a voltage range of 3.2-5.0 V. All the samples exhibit two similar plateaus at about 4.7 V and a small sloping plateau centered at 4.0 V, indicating that the products obtained have a space group of  $Fd-3m$ .<sup>39, 40</sup> The former plateaus are ascribed to the  $\text{Ni}^{2+}/\text{Ni}^{4+}$  redox couple, while the latter is associated with  $\text{Mn}^{3+}/\text{Mn}^{4+}$  redox couple. This result demonstrates that the  $\text{Li}_2\text{TiO}_3$  surface modification does not change the inherent charge and discharge behaviors of LNMO electrode, consistent with the XRD data. The initial discharge capacity of pristine LNMO is  $132 \text{ mAh g}^{-1}$ . After 3 wt. % and 5 wt. %  $\text{Li}_2\text{TiO}_3$  coating, the discharge capacities are  $128 \text{ mAh g}^{-1}$  and  $126 \text{ mAh g}^{-1}$ , respectively. However, the sample LNMO@LTO 10%

appears a severe capacity loss with a discharge capacity of 115  $\text{mAh g}^{-1}$ , which is likely due to the thick coating layer seriously impedes the electron transfer of LNMO. Moreover, it is distinct that the voltage difference between charge and discharge plateaus becomes smaller after 3 wt. % or 5 wt. %  $\text{Li}_2\text{TiO}_3$  coating, suggesting that the moderate  $\text{Li}_2\text{TiO}_3$  coating can be beneficial to reduce the polarization and internal resistance of the cells. In addition, some amount of  $\text{Ti}^{4+}$  ions doping could also improve electrochemical activity of LNMO.

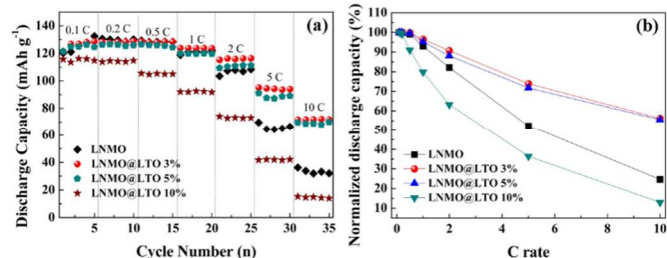
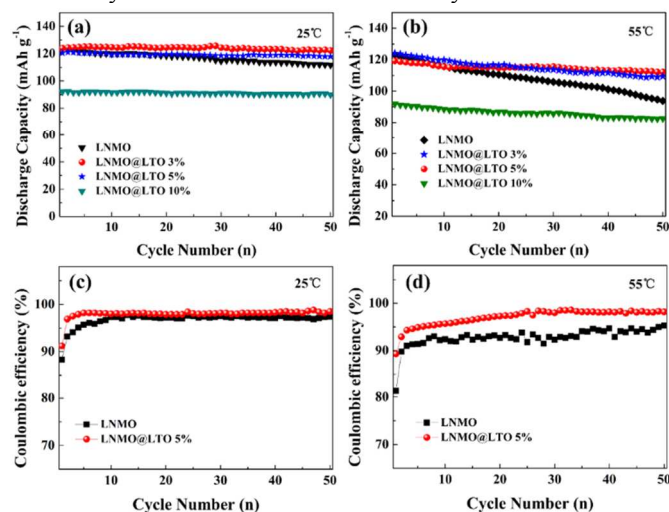


**Figure 5.** Rate performance for LNMO and LNMO@LTO at 25 °C.

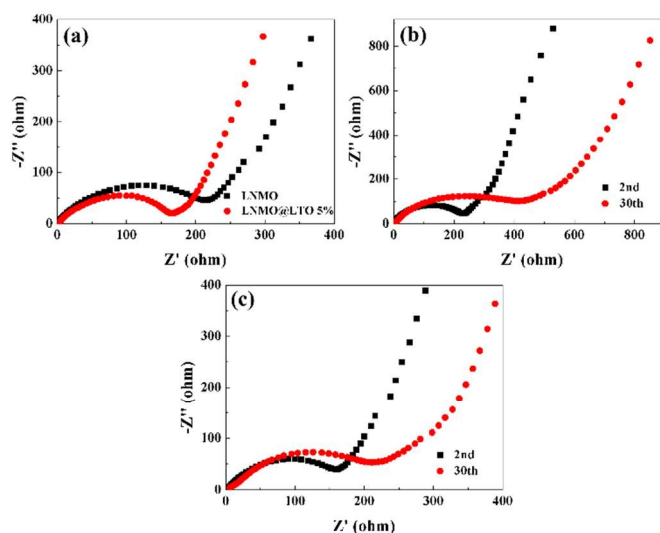
For the purpose of determining the influence of coating layer on rate performance of LNMO cathode materials, all the samples were cycled at different charge/discharge rates (0.1, 0.2, 0.5, 1, 2, 5, and 10 C) at room temperature. As shown in Figure 5a, compared to pristine LNMO electrode,  $\text{Li}_2\text{TiO}_3$ -modified LNMO@LTO electrodes show no evident difference in capacity at a lower discharging rate below 1 C, apart from the LNMO@LTO 10% sample which endured rapidly capacity loss from 0.1 C to 10 C rates. However, when the cells were charged and discharged at larger current densities of 2 C, 5 C, and 10 C, LNMO@LTO 3% and LNMO@LTO 5% still exhibit excellent rate capability while the pristine sample undergoes serious capacity fading. Particularly, at higher current rates of 5 C and 10 C, both LNMO@LTO 3% and LNMO@LTO 5% show considerably higher discharge capacities of 95 and 72  $\text{mAh g}^{-1}$  for the former and 90 and 70  $\text{mAh g}^{-1}$  for the latter. However, the pristine sample only delivered capacities of 70 and 35  $\text{mAh g}^{-1}$  at the same rates. To illustrate the differences in a clearer manner between the pristine and coated samples, we normalized the discharge capacity values at various C rates to the discharge capacity value at a 0.1 C rate and plotted in Figure 5b. It is obviously observed that the coated samples with 3 wt. % and 5 wt. %  $\text{Li}_2\text{TiO}_3$  show much better capacity retention than the bare one. At large current density of 5 C, the LNMO@LTO 3% and LNMO@LTO 5% can still sustain 73.9% and 71.8% capacity retention of 0.1 C rate, while the bare LNMO is only 52.2%. The above results indicate that proper amount of  $\text{Li}_2\text{TiO}_3$ -surface modification can significantly improve the rate performance of LNMO spinel.

Figure 6a, b compares the cyclability of the bare and surface modified LNMO samples at 1 C rate at different temperatures. At 25 °C, all the samples exhibit excellent cycle performance with the capacity retention of over 90% after repeated discharge-charge up to 50 cycles. However, at 55 °C, the first discharge capacity of bare LNMO is 122  $\text{mAh g}^{-1}$ , while it decreased to 94  $\text{mAh g}^{-1}$  after 50 cycles with only 77.1% capacity retention. Gratifyingly, through surface modifications, all the samples of LNMO@LTO show better capacity retention after 50 cycles at 55 °C than the bare one. The capacity retentions of LNMO@LTO 3%, LNMO@LTO 5% and LNMO@LTO 10% are 88.1%, 94.1% and 90.2%, respectively. Therefore, the  $\text{Li}_2\text{TiO}_3$ -surface modification offers an effective manner to remarkably improve the cyclability of LNMO cathode at elevated temperature. The Coulombic

efficiency (defined as the ratio of discharge to charge capacity) evolution during cyclic process of bare LNMO and LNMO@LTO 5% was shown in Figure 6c, d. At 25 °C, the average Coulombic efficiency of both samples are above 95%. When the temperature increased to 55 °C, the performance of  $\text{Li}_2\text{TiO}_3$ -modified electrodes did not show apparent decline while the bare electrode distinctly reduced to about 93%. The results suggest that the  $\text{Li}_2\text{TiO}_3$ -coatings could effectively alleviate reactions from electrolyte oxidation.<sup>41</sup>



**Figure 6.** Cycling performance for LNMO and LNMO@LTO at 25 °C (a) and 55 °C (b); Coulombic efficiency for LNMO and LNMO@LTO 5% at 25 °C (c) and 55 °C (d).



**Figure 7.** Electrochemical impedance spectra (EIS) of (a) the bare and LNMO@LTO 5% samples after the 5th cycle at 25 °C; (b) the bare sample after the 2nd and 30th cycle at 55 °C; the LNMO@LTO 5% sample after the 2nd and 30th cycle at 55 °C.

To further understand the difference in the electrochemical performances and polarization behaviors between the bare and the surface-modified samples, the pristine LNMO and LNMO@LTO 5% were analyzed by electrochemical impedance spectroscopy (EIS) after 5th cycle at 25 °C and 2nd, 30th at 55 °C. All the cells were in a stable open-circuit voltage value before the EIS measurements. Figure 7a shows the AC impedance test results for pristine LNMO and LNMO@LTO

5% after 5th cycle at 25 °C. It can be clearly seen that the charge transfer of LNMO@LTO 5% is much smaller than that of the uncoated sample. This result indicates that  $\text{Li}_2\text{TiO}_3$  as coating layer can effectively reduce the obstacle for  $\text{Li}^+$ -ion transfer at the electrode/electrolyte interface. Thus, the rate performance of LNMO is significantly enhanced with proper amount of  $\text{Li}_2\text{TiO}_3$  coated. It may be attributed to that  $\text{Li}_2\text{TiO}_3$  is a favorable  $\text{Li}^+$  conductor and could offer three-dimensional channels for  $\text{Li}^+$ -ion transmission, also LNMO was doped by some amount of  $\text{Ti}^{4+}$  ions.<sup>30</sup> As Figure 7b and 7c shown, after 30 cycles at 55 °C, the bare sample appears drastic increase in battery impedance compared to that at 2nd cycle, while that of LNMO@LTO 5% is of relatively weak increase. It could be ascribed to that  $\text{Li}_2\text{TiO}_3$ -surface modification can effectively restrain the side-reactions between cathode and electrolyte, thus the increase of charge transfer is observably slowed down.<sup>17-18</sup> Hence,  $\text{Li}_2\text{TiO}_3$  surface modification could be capable to improve the cyclability of LNMO cathode at high cutoff voltage and elevated temperature.

The schematic diagram of the  $\text{Li}_2\text{TiO}_3$ -coated LNMO composite and the mechanism of its role as  $\text{Li}^+$ -conductive cladding layer to inhibit the unfavorable interfacial side reactions are presented in Figure 8. As previous literature reports,  $\text{Ni}^{4+}$  ions formed at the charged state of the cathode ( $\text{Li}_{1-x}\text{Ni}_{0.5}\text{Mn}_{1.5}\text{O}_4$ ) is active to liquid electrolyte and can induce the oxidative degradation of electrolyte, which is the objective reason to the capacity fading of LNMO during cycle process at high temperature.<sup>24,25</sup> In this work,  $\text{Li}_2\text{TiO}_3$  as a protecting skin observably suppresses the electrolyte decomposition on electrode/electrolyte interface and thereby improves the capacity retention during iterative charge-discharge cycles.<sup>42,43</sup> Moreover, unlike oxide coatings which may hinder the transportation of  $\text{Li}^+$ ,  $\text{Li}_2\text{TiO}_3$  could offer a three-dimensional path for  $\text{Li}^+$  and the tempo of  $\text{Li}^+$ -transfer is improved, enhancing the rate capability of LNMO.

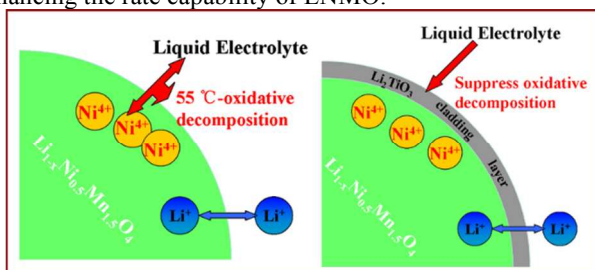


**Figure 8.** Schematic illustrations of the  $\text{Li}_2\text{TiO}_3$ -coated LNMO and its role as a  $\text{Li}^+$ -conductive cladding layer to inhibit the unfavorable interfacial side reactions.

As reported previously, the failure of LNMO cells could be mainly attributed to transition metal dissolution and diffusion to the anode leading to the damage to solid electrolyte interface (SEI) of anode and the cell impedance increase associated with oxidative decomposition of electrolyte.<sup>44, 45</sup> Surface coating which can stabilize the surface structure of cathode materials and mitigate metal-ion dissolution has been considered as one of the most effectively manners to ameliorate the electrochemical performance of the spinel and promote its practical application.<sup>41, 46</sup> In our work,  $\text{Li}^+$ -conductive  $\text{Li}_2\text{TiO}_3$  was employed to coat on the surface of LNMO cathode. As a protective layer, it could effectively reduce transition metal dissolution of LNMO and suppress the side reaction between electrode and electrolyte.

#### 4. Conclusions

In summary, a series of  $\text{Li}_2\text{TiO}_3$ -surface modified nanoparticles have been prepared by in situ hydrolysis followed by lithiation approach. The electrochemical performance of spinel LNMO cathode was significantly enhanced by exploiting nanoscale  $\text{Li}_2\text{TiO}_3$  layer. The obtained lithium ion conductor not only provides facile ion transport channels, effectively reducing the barrier for lithium ion transfer at the electrode/electrolyte interface, but also suppresses the formation of thick CEI layers during the charge-discharge process. This resultant material exhibits a remarkable rate capability, extremely high capacity, and excellent cycling ability, which may make LNMO materials very attractive for use in batteries for electric vehicles and grid-scale energy storage.

#### Acknowledgements

This work is financially supported by the National Program on Key Basic Research Project of China (973 Program, No. 2014CB239701), National Natural Science Foundation of China (No. 21173120, 51372116), Natural Science Foundations of Jiangsu Province (No. BK2011030), Fundamental Research Funds for the Central Universities of NUA (NP2014403), Funding for Outstanding Doctoral Dissertation in NUA (No. BCXJ14-12), and Funding of Jiangsu Innovation Program for Graduate Education (No. KYLX\_0254).

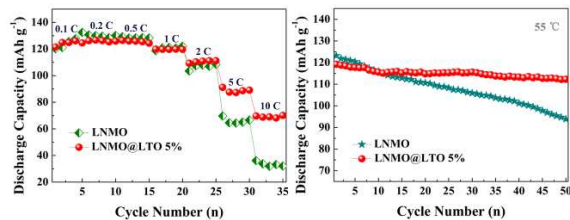
#### Notes and references

College of Material Science and Engineering, Key Laboratory for Intelligent Nano Materials and Devices of Ministry of Education, Nanjing University of Aeronautics and Astronautics, Nanjing, China. Fax: +86 025 52112626; Tel: +86 025 52112918; E-mail: azhangxg@163.com  
Group website: <http://xgzhang.nuaa.edu.cn/>  
Electronic Supplementary Information (ESI) available: [Supplementary table and figure]. See DOI: 10.1039/b000000x/

- Z. Li, Z. Xu, X. Tan, H. Wang, C. M. B. Holt, T. Stephenson, B. C. Olsen and D. Mitlin, *Energy Environ. Sci.*, 2013, **6**, 871-878.
- P. G. Bruce, S. A. Freunberger, L. J. Hardwick and J.-M. Tarascon, *Nat Mater*, 2012, **11**, 19-29.
- W.-K. Shin, Y.-S. Lee and D.-W. Kim, *J. Mater. Chem. A*, 2014, **2**, 6863-6869.
- L. Zhang, L. Zhou, H. B. Wu, R. Xu and X. W. Lou, *Angew. Chem. Int. Ed.*, 2012, **51**, 7267-7270.
- J. Lee, A. Urban, X. Li, D. Su, G. Hautier and G. Ceder, *Science*, 2014, **343**, 519-522.
- J. Ding, H. Wang, Z. Li, A. Kohandehghan, K. Cui, Z. Xu, B. Zahiri, X. Tan, E. M. Lotfabad, B. C. Olsen and D. Mitlin, *ACS Nano*, 2013, **7**, 11004-11015.
- D. Liu, B. B. Garcia, Q. Zhang, Q. Guo, Y. Zhang, S. Sepelri and G. Cao, *Adv. Funky. Mater.*, 2009, **19**, 1015-1023.
- A. Kraysberg and Y. Ein-Eli, *Adv. Eng. Mater.*, 2012, **2**, 922-939.
- P. Nie, L. Shen, F. Zhang, L. Chen, H. Deng and X. Zhang, *CrystEngComm*, 2012, **14**, 4284-4288.
- B. Xu, C. R. Fell, M. Chi and Y. S. Meng, *Energy Environ. Sci.*, 2011, **4**, 2223-2233.

11. L. Zhou, D. Zhao and X. Lou, *Angew. Chem., Int. Ed.*, 2012, **51**, 239-241.
12. A. Manthiram, K. Chemelewski and E.-S. Lee, *Energy Environ. Sci.*, 2014, **7**, 1339-1350.
13. J. Liu, W. Liu, S. Ji, Y. Zhou, P. Hodgson and Y. Li, *ChemPlusChem*, 2013, **78**, 636-641.
14. J. Feng, Z. Huang, C. Guo, N. A. Chernova, S. Upreti and M. S. Whittingham, *ACS Appl. Mater. Interfaces*, 2013, **5**, 10227-10232.
15. P. Reale, S. Panero and B. Scrosati, *J. Electrochem. Soc.*, 2005, **152**, A1949-A1954.
16. C. J. Jafra, M. K. Mathe, N. Manyala, W. D. Roos and K. I. Ozoemena, *ACS Appl. Mater. Interfaces*, 2013, **5**, 7592-7598.
17. H. Duncan, D. Duguay, Y. Abu-Lebdeh and I. J. Davidson, *J. Electrochem. Soc.*, 2011, **158**, A537-A545.
18. D. Aurbach, B. Markovsky, Y. Talyossef, G. Salitra, H.-J. Kim and S. Choi, *J. Power Sources*, 2006, **162**, 780-789.
19. B. Li, L. Xing, M. Xu, H. Lin and W. Li, *Electrochem. Commun.*, 2013, **34**, 48-51.
20. Z. Zhang, L. Hu, H. Wu, W. Weng, M. Koh, P. C. Redfern, L. A. Curtiss and K. Amine, *Energy Environ. Sci.*, 2013, **6**, 1806-1810.
21. N. P. W. Pieczonka, L. Yang, M. P. Balogh, B. R. Powell, K. Chemelewski, A. Manthiram, S. A. Krachkovskiy, G. R. Goward, M. Liu and J.-H. Kim, *J. Phys. Chem. C*, 2013, **117**, 22603-22612.
22. Y. K. Sun, K. J. Hong, J. Prakash and K. Amine, *Electrochem. Commun.*, 2002, **4**, 344-348.
23. D. Liu, Y. Bai, S. Zhao and W. Zhang, *J. Power Sources*, 2012, **219**, 333-338.
24. D. W. Shin, C. A. Bridges, A. Huq, M. P. Paranthaman and A. Manthiram, *Chem. Mater.*, 2012, **24**, 3720-3731.
25. D. Liu, J. Hamel-Paquet, J. Trotter, F. Barray, V. Gariépy, P. Hovington, A. Guerfi, A. Mauger, C. M. Julien, J. B. Goodenough and K. Zaghib, *J. Power Sources*, 2012, **217**, 400-406.
26. J.-H. Cho, J.-H. Park, M.-H. Lee, H.-K. Song and S.-Y. Lee, *Energy Environ. Sci.*, 2012, **5**, 7124-7131.
27. F. Cheng, Y. Xin, Y. Huang, J. Chen, H. Zhou and X. Zhang, *J. Power Sources*, 2013, **239**, 181-188.
28. M. Vijayakumar, S. Kerisit, Z. Yang, G. L. Graff, J. Liu, J. A. Sears, S. D. Burton, K. M. Rosso and J. Hu, *J. Phys. Chem. C*, 2009, **113**, 20108-20116.
29. X. Wu, Z. Wen, X. Xu and J. Han, *Solid State Ionics*, 2008, **179**, 1779-1782.
30. J. Lu, Q. Peng, W. Wang, C. Nan, L. Li and Y. Li, *J. Am. Chem. Soc.*, 2013, **135**, 1649-1652.
31. X. Yang, R. Yu, L. Ge, D. Wang, Q. Zhao, X. Wang, Y. Bai, H. Yuan and H. Shu, *J. Mater. Chem. A*, 2014, **2**, 8362-8368.
32. J. C. Arrebola, A. Caballero, M. Cruz, L. Hernán, J. Morales and E. R. Castellón, *Adv. Funct. Mater.*, 2006, **16**, 1904-1912.
33. K. M. Shaju and P. G. Bruce, *Dalton Trans.*, 2008, 5471-5475.
34. T. Fehr and E. Schmidbauer, *Solid State Ionics*, 2007, **178**, 35-41.
35. R. Alcántara, M. Jaraba, P. Lavela, J. L. Tirado, P. Biensan, A. de Guibert, C. Jordy and J. P. Peres, *Chem. Mater.*, 2003, **15**, 2376-2382.
36. M. Lin, S. H. Wang, Z. L. Gong, X. K. Huang and Y. Yang, *J. Electrochem. Soc.*, 2013, **160**, A3036-A3040.
37. E. Memarzadeh Lotfabad, P. Kalisvaart, K. Cui, A. Kohandehghan, M. Kupsta, B. Olsen and D. Mitlin, *Phys. Chem. Chem. Phys.*, 2013, **15**, 13646-13657.
38. A. Kohandehghan, P. Kalisvaart, K. Cui, M. Kupsta, E. Memarzadeh and D. Mitlin, *J. Mater. Chem. A*, 2013, **1**, 12850-12861.
39. J. Liu and A. Manthiram, *J. Phys. Chem. C*, 2009, **113**, 15073-15079.
40. E. Lee and K. A. Persson, *Energy Environ. Sci.*, 2012, **5**, 6047-6051.
41. J. S. Park, X. Meng, J. W. Elam, S. Hao, C. Wolverton, C. Kim and J. Cabana, *Chem. Mater.*, 2014, **26**, 3128-3134.
42. X. Meng, X.-Q. Yang and X. Sun, *Adv. Mater.*, 2012, **24**, 3589-3615.
43. J. Li, L. Baggetto, S. K. Martha, G. M. Veith, J. Nanda, C. Liang and N. J. Dudney, *Adv. Eng. Mater.*, 2013, **3**, 1275-1278.
44. D. Lu, M. Xu, L. Zhou, A. Garsuch and B. L. Lucht, *J. Electrochem. Soc.*, 2013, **160**, A3138-A3143.
45. X. Xiao, D. Ahn, Z. Liu, J.-H. Kim and P. Lu, *Electrochem. Commun.*, 2013, **32**, 31-34.
46. J. Chong, S. Xun, J. Zhang, X. Song, H. Xie, V. Battaglia and R. Wang, *Chem. Eur. J.* 2014, **20**, 1-8.

## Entry for the Table of Contents



High-voltage  $\text{LiNi}_{0.5}\text{Mn}_{1.5}\text{O}_4$  cathode was surface-modified by  $\text{Li}^+$ -conductive  $\text{Li}_2\text{TiO}_3$  and proper amount of  $\text{Li}_2\text{TiO}_3$  can significantly improve the lithium storage capability.